

# Effect of 3*p*- and 5*d*-electron doping on the Kondo Semiconductor CeFe<sub>2</sub>Al<sub>10</sub>

Rajesh Tripathi<sup>1,2</sup>, D T Adroja<sup>1,3</sup>, M R Lees<sup>4</sup>, V K Anand<sup>5,6</sup>, A Sundaresan<sup>2</sup>, S Langridge<sup>1</sup>, A Bhattacharyya<sup>7</sup>, Y Muro<sup>8</sup>, K Hayashi<sup>9</sup>, T Takabatake<sup>9</sup>

<sup>1</sup>ISIS Facility, STFC, Rutherford Appleton Laboratory, Chilton, Oxon OX11 0QX, United Kingdom

<sup>2</sup>Jawaharlal Nehru Centre for Advanced Scientific Research, Jakkur, Bangalore 560064, India

<sup>3</sup>Highly Correlated Matter Research Group, Physics Department, University of Johannesburg, P.O. Box 524, Auckland Park 2006, South Africa

<sup>4</sup>Department of Physics, University of Warwick, Coventry CV4 7AL, UK

<sup>5</sup>Helmholtz-Zentrum Berlin für Materialien und Energie GmbH, Hahn-Meitner Platz 1, D-14109 Berlin, Germany

<sup>6</sup>University of Petroleum and Energy Studies, Dehradun, Uttarakhand, 248007, India

<sup>7</sup>Department of Physics, Ramakrishna Mission Vivekananda Educational and Research Institute, Belur Math, Howrah 711202, West Bengal, India

<sup>8</sup>Liberal Arts and Sciences, Faculty of Engineering, Toyama Prefectural University, Imizu 939-0398, Japan

<sup>9</sup>Graduate School of Advanced Science and Engineering, Hiroshima University, Higashi-Hiroshima 739-8530, Japan

E-mail: rajeshtripathi@jncasr.ac.in, devashibhai.adroja@stfc.ac.uk

**Abstract.** We examined the effect of 3*p*- and 5*d*-electron doping on the Kondo semiconductor CeFe<sub>2</sub>Al<sub>10</sub> by means of the electrical resistivity ( $\rho$ ), magnetic susceptibility ( $\chi$ ), and specific heat ( $C$ ) measurements. The results show that in the 3*p*-electron-doped system CeFe<sub>2</sub>Al<sub>10-y</sub>Si<sub>y</sub>, the semiconducting behavior is suppressed for  $y = 0.05$ , and the system adopts a metallic ground state with an increase in the density of states at the Fermi level. The Si substitution leads to a large decrease in the paramagnetic Weiss temperature  $\theta_P$  indicating a reduction in *c-f* hybridization strength, however the Si does not induce magnetic order up to  $y = 0.3$  down to 2 K. The systematic changes in  $\rho(T)$ ,  $\chi(T)$ , and  $C(T)$  are similar to those for 5*d*-electron doped system CeFe<sub>2-x</sub>Ir<sub>x</sub>Al<sub>10</sub>, although, Ir substitution induces a bulk antiferromagnetic transition below 3.1 K in CeFe<sub>1.7</sub>Ir<sub>0.3</sub>Al<sub>10</sub>. These changes can be explained by the collapse of the hybridization gap due to the suppression of the *c-f* hybridization effect. Our results further confirm that the collapse of the spin/charge gap by an excess electron doping is one of the universal features of the Kondo semiconductors CeT<sub>2</sub>Al<sub>10</sub> ( $T = \text{Fe, Ru, and Os}$ ).

## 1. Introduction

The Kondo semiconductors CeT<sub>2</sub>Al<sub>10</sub> ( $T = \text{Fe, Ru, and Os}$ ) have been studied intensively as the compounds with  $T = \text{Ru and Os}$  exhibit antiferromagnetic (AFM) phase transitions at unusually high temperature ( $T_N = 27.3$  and 28.7 K, with a very low ordered state moment  $\mu \simeq 0.40$  and  $0.29 \mu_B/\text{Ce}$  for  $T = \text{Ru and Os}$ , respectively) despite the Ce-Ce distances of more than 5 Å in the cagelike orthorhombic crystal structure [1]. Surprisingly, these  $T_N$  values are much higher



than those in the isostructural gadolinium compounds  $\text{GdT}_2\text{Al}_{10}$  ( $T_N = 17.5$  K for  $T = \text{Ru}$  and 18 K for  $T = \text{Os}$  with  $\mu \simeq 7\mu_B$ ) [2]. Optical conductivity measurements on  $\text{CeT}_2\text{Al}_{10}$  ( $T = \text{Ru}$  and  $\text{Os}$ ) have revealed that a charge-density-wave-like instability develops along the  $b$  axis at temperatures slightly higher than  $T_N$  which induces unconventional AFM ordering [3]. Furthermore,  $\text{CeT}_2\text{Al}_{10}$  with  $T = \text{Fe}$ , exhibits semiconducting behavior with nonmagnetic ground state down to 45 mK [4]. Indeed, the temperature dependent resistivity obeys the thermal activation-type form  $\rho(T) \propto \exp(\Delta/k_B T)$ , for  $T < 20$  K, exhibiting a semiconducting behavior. The temperature dependence of the magnetic susceptibility suggests an intermediate valence behavior for  $\text{CeFe}_2\text{Al}_{10}$  with a strong magnetic anisotropy owing to the strong  $c$ - $f$  hybridization [4]. The optical conductivity measurements on  $\text{CeFe}_2\text{Al}_{10}$  at low temperatures, have revealed an optical transition across the hybridization gap between the conduction band and the localized  $4f$  states, namely  $c$ - $f$  hybridization, appears at 55 meV [5]. Due to the highest degree of  $c$ - $f$  hybridization,  $\text{CeFe}_2\text{Al}_{10}$  is expected to have the largest real gap or pseudogap feature among the  $\text{CeT}_2\text{Al}_{10}$  ( $T = \text{Fe}, \text{Ru}, \text{Os}$ ) materials [5].

In the present study, we have observed marked changes in the thermal and transport properties of  $\text{CeFe}_2\text{Al}_{10}$  induced by  $3p$  (Si for Al)- and  $5d$  (Ir for Fe)-electron doping. The low-temperature energy gap, which is proposed to be a consequence of strong  $c$ - $f$  hybridization is suppressed by a small amount of Si/Ir substitution, and the system adopts a metallic ground state with an increase in the density of states at the Fermi level. With increasing Ir concentration  $x$  in  $\text{CeFe}_{2-x}\text{Ir}_x\text{Al}_{10}$ , the system undergoes long-range AFM order below 3.1 K for  $x = 0.3$ . On the contrary, Si substitution does not induce magnetic order up to  $y = 0.3$  down to 2 K. The emergence of AFM order in  $\text{CeFe}_{1.7}\text{Ir}_{0.3}\text{Al}_{10}$  was attributed to the combined effect of weakening of  $c$ - $f$  exchange interaction and the lattice contraction along the  $b$  axis [6].

## 2. Experimental details

Polycrystalline samples of  $\text{CeFe}_2\text{Al}_{10-y}\text{Si}_y$  ( $y = 0.1, 0.2, 0.3$ ), and  $\text{CeFe}_{2-x}\text{Ir}_x\text{Al}_{10}$  ( $x = 0, 0.08, 0.16, 0.3$ ) were prepared by standard arc melting of stoichiometric quantities of high purity elements. The obtained ingots were then annealed for a week at 1000 °C. Powder x-ray diffraction confirmed the  $\text{YbFe}_2\text{Al}_{10}$ -type orthorhombic structure (space group  $Cmcm$ ) [Fig. 1(a)]. The crystal structures were refined by the Rietveld method and the lattice parameters as a function of the  $x$  and  $y$  are shown in Fig. 1(a) and Fig. 1(b), respectively. All the samples were single phase except for the sample  $y = 0.3$ , containing a small amount of  $\text{CeAl}_{0.9}\text{Si}_{1.1}$ , which orders ferromagnetically with  $T_C = 11$  K [7]. The lattice parameters and hence unit cell volume of  $\text{CeFe}_2\text{Al}_{10-y}\text{Si}_y$  decreases with increasing  $y$ , while the lattice parameters exhibit anomalous changes for  $\text{CeFe}_{2-x}\text{Ir}_x\text{Al}_{10}$  such that the unit cell volume remains almost unchanged. The  $\rho(T)$  measurements were performed using a standard four-probe method using the resistivity option of a Quantum Design Physical Property Measurement System (PPMS). The  $C(T)$  was measured by the relaxation method in a PPMS. The  $\chi(T)$  was measured by using a commercial SQUID magnetometer in a magnetic field  $B = 0.1$  T.

## 3. Results and Discussion

Figure 2(a) shows the temperature dependence of electrical resistivity  $\rho(T)$  for  $\text{CeFe}_2\text{Al}_{10-y}\text{Si}_y$  ( $y = 0, 0.1, 0.2$ , and  $0.3$ ) down to 2 K. The  $\rho$  for  $y = 0$  increases with decreasing  $T$ , with a broad hump near  $T_{\text{coh}} = 75$  K and a sharp upturn below  $T = 20$  K. The low-temperature behavior is well described by the activation law,  $\rho(T) = \rho_0 \exp(\Delta/2k_B T)$ , presenting a typical Kondo semiconducting behavior. The  $-\ln T$  behavior above  $T_{\text{coh}}$  can be ascribed to Kondo scattering on the crystal field excited states. For  $y \geq 0.1$ , the Kondo semiconducting behavior below  $T = 20$  K abruptly disappears and  $\rho(T)$  becomes metallic at low temperature. A similar change in  $\rho(T)$  is also seen with  $x$  for  $\text{CeFe}_{2-x}\text{Ir}_x\text{Al}_{10}$  [Fig. 2(b)]. Therefore, the metallization in  $\text{CeFe}_2\text{Al}_{10}$  seems to be favored by both  $3p$  and  $5d$  electron doping. In Si-doped  $\text{CeFe}_2\text{Al}_{10-y}\text{Si}_y$ ,

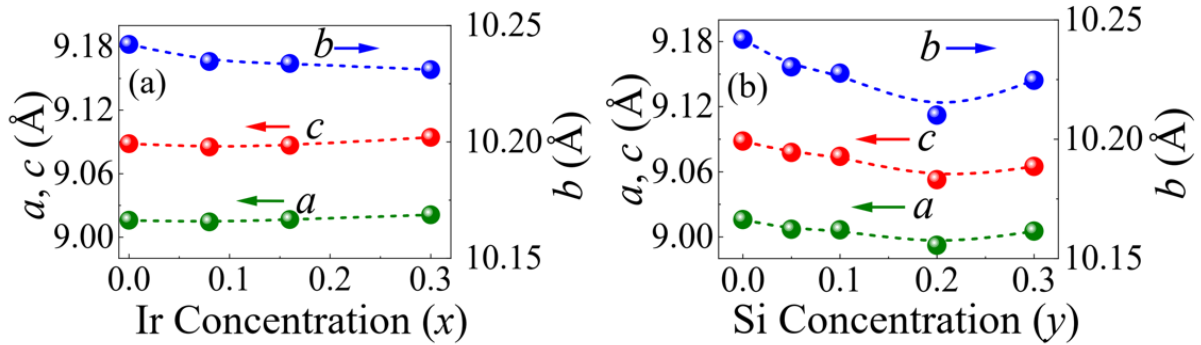


**Figure 1.** (a) The variation of the lattice parameters as a function of Ir concentration  $x$  for  $\text{CeFe}_{2-x}\text{Ir}_x\text{Al}_{10}$  (b) The variation of the lattice parameters as a function of Si concentration  $y$  for  $\text{CeFe}_2\text{Al}_{10-y}\text{Si}_y$ .

the low-temperature maximum in  $\rho$  at  $T_0 \sim 30$  K for  $y = 0.1, 0.2, 0.3$  can be attributed to the onset of Kondo coherence to the crystal field ground state and the high temperature  $-\ln T$  is the result of the Kondo scattering from the excited CEF states of  $\text{Ce}^{3+}$ . A similar feature in  $\rho(T)$  is also seen for  $\text{CeOs}_2\text{Al}_{10}$  where a metallic ground state has been realized with both electron (Ir/Rh) and hole (Re)-doping [12].

Figures 2(c) and 2(d) shows the temperature dependence of magnetic susceptibility  $\chi$  for  $\text{CeFe}_2\text{Al}_{10-y}\text{Si}_y$  and  $\text{CeFe}_{2-x}\text{Ir}_x\text{Al}_{10}$ . The low temperature  $\chi$  increases with increasing  $y$ , however, no signature of bulk magnetic ordering could be seen down to 2 K up to  $y = 0.3$ . The inverse susceptibility ( $\chi^{-1}$  vs  $T$ ) data for  $\text{CeFe}_2\text{Al}_{10-y}\text{Si}_y$  (not shown here) follow the Curie–Weiss like behavior at  $T > 100$  K. A least squares fit to the  $\chi(T)$  data above 100 K with the modified Curie–Weiss law yielded the effective magnetic moment  $\mu_{\text{eff}} = 2.32(4), 2.25(1), 2.20(3)$  and  $2.13(1) \mu_B/\text{Ce}$ , and paramagnetic Weiss temperatures  $\Theta_P$  of  $-377(6), -346(3), -147(1)$ , and  $-112(3)$  K for the samples with  $y = 0, 0.1, 0.2$ , and  $0.3$ , respectively. The estimated  $\mu_{\text{eff}}$  are slightly smaller than  $2.54 \mu_B$ , expected for a free  $\text{Ce}^{3+}$  ion. This discrepancy may be due to crystal-field effects. A large and negative value of  $\Theta_P$  is a common feature in Ce-based compounds with strong  $c-f$  hybridization [8]. The variation of  $|\Theta_P|$  with  $y$  for  $\text{CeFe}_2\text{Al}_{10-y}\text{Si}_y$  suggests that the Si substitution suppresses the  $c-f$  hybridization and leads to the localization of the Ce-4f electrons.

On the other hand, Ir substitution for Fe changes the system more strongly from the intermediate valence regime to a localized regime owing to the suppression of  $c-f$  hybridization. In fact,  $\chi(T)$  of  $\text{CeFe}_{2-x}\text{Ir}_x\text{Al}_{10}$  for  $x = 0.3$  exhibits a sharp peak at  $T = 3.1$  K [shown by an arrow in Fig. 2(d)], indicating a phase transition to an AFM ordered state, which was confirmed through a muon spin rotation study [6]. The previous studies on  $\text{CeT}_2\text{Al}_{10}$  ( $T = \text{Ru}, \text{Os}$ ), report a gap related to the charge- and spin-density waves along the  $b$  axis, in addition to a hybridization gap along all three axes [9]. It is also found that the application of uniaxial pressure along the  $b$  axis strongly enhanced the  $T_N$  of  $\text{CeT}_2\text{Al}_{10}$  ( $T = \text{Ru}, \text{Os}$ ) [10]. In  $\text{CeFe}_{1.7}\text{Ir}_{0.3}\text{Al}_{10}$  we have observed an anomalous change in the lattice parameters, in particular a contraction along the  $b$  axis, which may be taken as an effective uniaxial pressure in the system. This in addition to the weakening of the  $c-f$  hybridization gives rise to magnetic ordering in contrast to Si doping. Here it is important to note that the  $3p$  (Si)- and  $4d$  (Rh)-electron doping in  $\text{CeRu}_2\text{Al}_{10}$  play an equivalent role in both the formation of hybridization gap and the unusual AFM ordering [11]. The observed long-range ordered magnetic ground state with Ir substitution rather than the paramagnetic ground state seen with Si substitution could, therefore, be attributed to the combined effect of  $b$  axis behavior and weakens strength of the  $c-f$  hybridization.

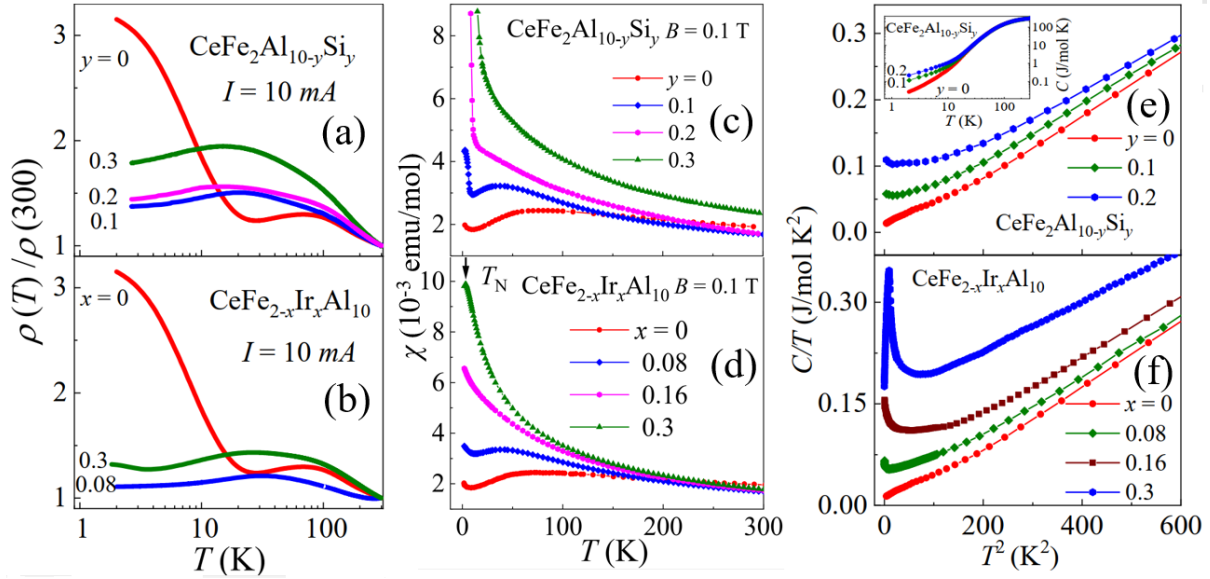


**Figure 2.** (a)  $T$  dependence of  $\rho$  for polycrystalline samples of CeFe<sub>2</sub>Al<sub>10-y</sub>Si<sub>y</sub>. (b)  $\rho(T)$  of CeFe<sub>2-x</sub>Ir<sub>x</sub>Al<sub>10</sub>. (c)  $\chi(T)$  for polycrystalline samples of CeFe<sub>2</sub>Al<sub>10-y</sub>Si<sub>y</sub>. (d)  $\chi(T)$  of CeFe<sub>2-x</sub>Ir<sub>x</sub>Al<sub>10</sub>. (e)  $C/T$  versus  $T^2$  for CeFe<sub>2</sub>Al<sub>10-y</sub>Si<sub>y</sub>. Inset: Heat capacity  $C(T)$  for polycrystalline samples of CeFe<sub>2</sub>Al<sub>10-y</sub>Si<sub>y</sub> on a log-log plot. (f)  $C/T$  versus  $T^2$  for CeFe<sub>2-x</sub>Ir<sub>x</sub>Al<sub>10</sub>.

The double logarithmic plot of heat capacity  $C$  versus  $T$  for CeFe<sub>2</sub>Al<sub>10-y</sub>Si<sub>y</sub> ( $y = 0, 0.1$ , and  $0.2$ ) are shown in the inset of Fig. 2(e). At  $T < 10$  K,  $C$  increases with increasing  $y$  without any sign of magnetic ordering, reminiscent of heavy-fermion-like behavior. On the other hand, for  $x = 0.3$  in CeFe<sub>2-x</sub>Ir<sub>x</sub>Al<sub>10</sub>, a  $\lambda$ -type anomaly is observed at  $T \sim 3$  K further indicating the onset of long-range AFM ordering. Figures 2(e) and 2(f) show the variation of  $C/T$  with  $T^2$  for CeFe<sub>2</sub>Al<sub>10-y</sub>Si<sub>y</sub> and CeFe<sub>2-x</sub>Ir<sub>x</sub>Al<sub>10</sub>, respectively. For  $y = 0$ ,  $C/T$  (or  $\gamma$ ) at 2 K is almost zero, suggesting a very small or zero density of states at the Fermi level. However, for  $y \geq 0$ ,  $\gamma$  is significantly enhanced and reaches 0.11 J/mole K<sup>2</sup> for  $y = 0.2$ . Similar behavior is also seen for CeFe<sub>2-x</sub>Ir<sub>x</sub>Al<sub>10</sub> [Fig. 2(f)]. In other  $T$ -site substituted systems e.g. Ce(Fe<sub>1-x</sub>Rh<sub>x</sub>)<sub>2</sub>Al<sub>10</sub>, Ce(Ru<sub>1-x</sub>Rh<sub>x</sub>)<sub>2</sub>Al<sub>10</sub> or Ce(Os<sub>1-x</sub>Ir<sub>x</sub>)<sub>2</sub>Al<sub>10</sub> [12], the  $\gamma$  value increases rapidly with  $x$ , which is attributed to a rapid collapse of a hybridization gap (or spin gap) and the appearance of conduction electrons with high effective mass at the Fermi level. We, therefore, anticipate that the enhancement of  $\gamma$  in the heat capacity of CeFe<sub>2</sub>Al<sub>10-y</sub>Si<sub>y</sub> and CeFe<sub>2-x</sub>Ir<sub>x</sub>Al<sub>10</sub> is associated with the appearance of a finite density of states close to the Fermi level. Support for this scenario comes from the behavior of the low temperature electrical resistivity. Thus, the above characteristic doping effect is common in all the CeT<sub>2</sub>Al<sub>10</sub> systems ( $T = \text{Fe, Ru, and Os}$ ) with both  $3p$  and  $4d/5d$ -electron doping.

#### 4. Conclusions

We have investigated the magnetic, thermal, and electronic transport properties of Si- and Ir-substituted Kondo semiconducting compound CeFe<sub>2</sub>Al<sub>10</sub> using  $\rho(T)$ ,  $\chi(T)$ , and  $C(T)$  measurements. In CeFe<sub>2</sub>Al<sub>10-y</sub>Si<sub>y</sub>, the localized nature of the Ce ion is much enhanced by Si doping. However, no bulk magnetic ordering is observed down to 2 K even up to  $y = 0.3$ . On the other hand, Ir substitution induces a bulk AFM transition below  $T_N = 3.1$  K in CeFe<sub>1.7</sub>Ir<sub>0.3</sub>Al<sub>10</sub>. The observed long-range ordered magnetic ground state with Ir substitution rather than the

paramagnetic ground state seen with Si substitution is attributed to the combined effect of changes in the  $b$  axis and a weakening of the  $c$ - $f$  hybridization. Our results further suggests that the electron doping achieved by substituting Fe with Ir (or Al with Si), weakens the  $c$ - $f$  hybridization and destroys the Kondo semiconducting character and the spin/charge gapped state at low temperatures.

### Acknowledgements

DTA would like to thank the Royal Society of London for the Newton Advanced fellowship funding between UK and China, and International Exchange funding between UK and Japan. DTA also thanks EPSRC UK for funding (grant ref. EP/W00562X/1). RT thanks the Indian Nanomission for a post-doctoral fellowship. Y. M and T. T acknowledge the financial supports from JSPS, grant numbers JP26400363, JP15K05180, JP16H01076, and JP21K03473.

### References

- [1] T. Nishioka, et al., J. Phys.Soc. Jpn. 78, 123705(2009); H. Kato, et al., J. Phys. Soc. Jpn. 80, 073701 (2011).
- [2] Y. Muro, et al., J. Phys. Soc. Jpn. 80, SA021 (2011).
- [3] S. I. Kimura, et al., Phys. Rev. Lett. 106, 056404 (2011).
- [4] Y. Muro, et al., J. Korean Phys. Soc. 63, 508 (2013); Y. Muro, et al., J. Phys. Soc. Jpn. 78, 083707 (2009); H. Tanida, et al., J. Phys. Soc. Jpn. 83, 084708 (2014).
- [5] S. Kimura<sup>1</sup>, et al., J. Phys. Soc. Jpn. 80, 033702 (2011); J. Kawabata, et al., Phys. Rev. B 92, 201113(R) (2015); D. T. Adroja, et al., Solid State Phenom. 257, 11 (2017).
- [6] R.Tripathi, et al., Phys. Rev. B. (accepted)(2021).
- [7] K. Hayashi, et al., J. Phys. Soc. Jpn. 85, 034714 (2016).
- [8] J. G. Sereni, et al., Phys. Rev. B 75, 024432 (2007).
- [9] S.-I. Kimura, et al., Phys. Rev. Lett. 106, 056404 (2011); Phys. Rev. B 91, 241120(R) (2015).
- [10] K. Hayashi, et al., Phys. Rev. B 96, 245130 (2017).
- [11] K. Hayashi, et al., J. Phys. Soc. Jpn. 85, 034714 (2016).
- [12] H. Tanida, et al., Phys. Rev. B 92, 235154 (2015); H. Tanida, et al., Phys. Rev. B 92, 235154 (2015); J. Kawabata, et al., Phys. Rev. B 89, 094404 (2014).